NASA Technical Memorandum 89820

Hot Corrosion Attack and Strength Degradation of SiC and Si_3N_4

(NASA-TM-89820) HOT CORROSION ATTACK AND STRENGTH DEGRADATION OF SiC AND Si(SUB)3N(SUB)4 (NASA) 12 p CSCL 11G

N87-20425

Unclas
G3/27 45387

James L. Smialek, Dennis S. Fox,
and Nathan S. Jacobson
Lewis Research Center
Cleveland, Ohio

Prepared for the
Environmental Degradation of Engineering Materials III
sponsored by Pennsylvania State University
University Park, Pennsylvania, April 13–15, 1987

NASA

HOT CORROSION ATTACK AND STRENGTH DEGRADATION OF SiC AND Si_3N_4

James L. Smialek, Dennis S. Fox, and Nathan S. Jacobson

National Aeronautics and Space Administration
Lewis Research Center
Cleveland, Ohio 44135

E-3466

SUMMARY

Thin films of Na_2SO_4 and Na_2CO_3 molten salt deposits were used to corrode sintered SiC and Si_3N_4 at 1000 °C. The resulting attack produced pitting and grain boundary etching resulting in strength decreases ranging from 15 to 50 percent. Corrosion pits were the predominant sources of fracture. The degree of strength decrease was found to be roughly correlated with the depth of the pit, as predicted from fracture toughness considerations. Gas evolution and bubble formation were key aspects of pit formation. Many of the observations of furnace exposures held true in a more realistic burner rig test.

INTRODUCTION

This paper is a companion to the previous paper which has described the chemical mechanisms of molten sodium salt corrosion of silicon-based ceramics. The major aspect of that work is that Na_2SO_4 and Na_2CO_3 salts react with SiC and Si_3N_4 in the presence of oxygen to form a liquid, nonprotective corrosion product of $Na_2O \cdot xSiO_2$ and gas evolution of CO, CO_2, or N_2 (ref. 1). The present paper summarizes the corrosion effects on the surface morphology and flexural strength as described in previous publications (refs. 2 to 5). The primary thrust is to show how this surface modification causes a commensurate and serious effect on residual strength.

EXPERIMENTAL PROCEDURE

The materials tested were commercially available sintered SiC and Si_3N_4 as listed in table I.

These materials are basically pressureless sintered ceramics with the exception of KX01 which is reaction sintered. Material A contains free carbon and B_4C used as sintering aids. Material C also employs boron and carbon as sintering aids. Material D contains residual free Si. Material E contains Al_2O_3 and Y_2O_3 as sintering aids. The test specimens were 1 in. flexure bars either machined or manually polished to about a 15 μm finish. For furnace testing the salt was first sprayed from a saturated water solution to a thickness of about 2 to 3 mg/cm^2. Burner rig testing was performed at a pressure of 4 atm (400 kPa), at a velocity of 95 m/sec, and at sodium doping levels of 2 and 4 ppm. Jet A fuel having 0.05 percent sulfur impurity was used. The attack morphologies were examined primarily by SEM after the corrosion products were dissolved in a 10 percent HF-H_2O solution. Flexural strengths were obtained in a four-point bend rig at a loading rate of 0.05 cm/min. The fracture origins were examined both before and after dissolution of the corrosion products.

RESULTS AND DISCUSSION

SiC

Furnace corrosion of SiC (A) by Na_2SO_4 in a 0.1 percent SO_2/O_2 atmosphere resulted in the most severe mode of attack. This occurred because of the synergistic effect of the free carbon in this material, i.e., very basic conditions at the melt-SiC interface, and excessive gas evolution of SO_3 and CO. The material was severely etched by hot corrosion as shown in figure 1 for a sample whose corrosion products were removed by HF dissolution. Corrosion in Na_2SO_4/air and Na_2CO_3/CO_2 environments produced somewhat less severe attack morphologies. These exposures resulted in shallower pits than those in figure 1 and regions that showed grain boundary etching rather than pitting.

The results of the flexural tests on the as-received and corroded materials are shown in figure 2. Considerable strength reductions occurred for the Na_2SO_4 exposures which were statistically significant at the 95 percent level according to the t-test. The Na_2CO_3 exposure produced a large scatter band due to the wide distributions in pit morphology and was not significantly lower than the as-received strength.

A typical fracture origin for SiC (A) is shown in figure 3 for Na_2SO_4/SO_3 corrosion. Note that the honeycomb-like pit is the center of the crack pattern and exhibits the complex pit-SiC interface. A detail of a fracture origin from a duplicate sample is shown in figure 4. Here the interface is revealed before and after HF dissolution of the corrosion products. Note that a gas bubble was present in the oxide very close to the SiC. This was a common observation and will be related to the mechanism of pitting later.

The strength of SiC should be governed by the criterion for brittle failure:

$$\sigma_f = \frac{ZK_{Ic}}{Ya^{1/2}} \qquad (1)$$

where Z and Y are flaw shape and geometry factors, K_{Ic} is fracture toughness (2.8 MPa $\cdot$ $m^{1/2}$), and "a" is the depth of an atomically sharp semicircular critical flaw. Although this definition of the critical flaw does not strictly apply to the pits causing failure, a reasonable correlation between strength and pit depth was found (fig. 5). The average value of K_{Ic} determined from this data was 2.6 MPa $\cdot$ $m^{1/2}$ and was very close to the independently determined value. This correlation and agreement show that the size of the corrosion pits controls the degree of strength degradation.

Burner rig exposures also caused considerable strength reductions of this and other SiC materials, figure 6. The morphology and chemistry of the corrosion product and the degree of strength reduction were most similar to those produced by Na_2SO_4/air furnace exposures. One major difference was that the burner rig supplied continuous deposition of Na_2SO_4 resulting in thicker Na2O$\cdot$xSiO2 liquid layers. The high gas velocities forced this viscous product toward the trailing edges and caused more extensive surface recession (20 μm) as compared to the leading edge (<5 μm). However the size of the pits was much greater at the leading edge as shown by the montage across the width of a specimen surface (fig. 7). A limited amount of fractography showed that

similar corrosion pit fracture origins existed for materials A, B, C, and D. Also the depth of the pits causing failure in material A agreed with the amount of strength degradation according to equation (1), giving an average K_{Ic} of 3.3 MPa • $m^{1/2}$.

Si_3N_4

The preliminary results for Si_3N_4 show somewhat similar behavior to those for SiC. Strength reductions on the order of 25 to 30 percent were observed for materials E, F, and G in burner rig tests (fig. 8). The reduction for a Na_2SO_4/O_2 furnace test of material E was similar to that of the rig test, however the different batch of material resulted in a different as-received strength.

The precise attack morphology at the $Na_2O{\cdot}xSiO_2$ - Si_3N_4 interface has not been examined as successfully as the SiC case. HF dissolution of the corrosion products was also found to attack the oxide grain boundary phases (Al, Y silicates) such that some Si_3N_4 grains were also removed. However fractography of non-HF treated samples did reveal that the failure origins were in regions where arrays of gas bubbles had existed. Also bubbles were often located within the scale at the origin (fig. 9). The depth of pitting appeared minimal for the furnace specimens, about 10 to 20 μm. However the burner rig samples showed more evidence of pitting, amounting to 20 to 60 μm.

Pitting

Clearly, pitting was the major mode of attack for SiC and was probably important for Si_3N_4 as well. Understanding this attack mode is therefore critical to understanding the root cause of strength reduction in the hot corrosion of ceramics. One of the major factors in pit formation on SiC was found to be the formation of gas bubbles and the disruption of the protective inner layer of SiO_2 that eventually forms as the Si/Na ratio increases during corrosion.

An example of this disrupted film is shown in figure 10 for material A after just 1 hr of corrosion. Here the water soluble $Na_2O{\cdot}xSiO_2$ outer scale has been dissolved away leaving only the inner SiO_2 layer. The holes were regions where bubbles existed, allowing continued corrosion of the SiC by the nonprotective $Na_2O{\cdot}xSiO_2$ liquid scale. Thus corrosion persisted in these regions while the adjacent areas were protected. The location of pits in the SiC directly beneath these holes is clearly evident. We therefore maintain that gaseous corrosion products (CO, CO_2, SO_3, and N_2) and bubble formation are the key factors in producing the crater-like strength-controlling pits. The situation for Si_3N_4 has not been as clearly defined at this time. Degradation of the grain boundary oxide by Na may be an additional factor here.

Other types of pitting appear to be innate to Si-base materials in the presence of molten salts. For example, single crystal SiC has no excess carbon and therefore a reduced potential for CO bubble formation. It also has no grain boundaries which would serve as preferential etching sites. Single crystal Si has no carbon whatsoever and no potential for gaseous corrosion products. Nevertheless both materials showed evidence of pitting by Na_2CO_3 corrosion (fig. 11). In these cases the pits were crystallographic in nature,

much finer than the bubble-induced pitting, and less frequent in the semiconductor grade (dislocation-free) Si.

SUMMARY AND CONCLUSIONS

Na_2SO_4 and Na_2CO_3 corrosion of SiC and Si_3N_4 has resulted in surface degradation due to pitting attack. The most detrimental type of pitting was associated with bubble formation and disruptions in the inner SiO_2 layer for SiC materials. A lesser degree of pitting was observed for Si_3N_4. The strength degradation ranged from 15 to 50 percent for SiC and 25 to 35 percent for Si_3N_4 depending on the specific material and exposure condition. Burner rig exposures produced similar results and conclusions to those of the furnace tests, with the potential for greater total amounts of sulfate deposition, scale formation, and surface recession. These studies indicate that the conditions of sodium ingestion and Na_2SO_4 deposition must be avoided for heat engines intending to utilize high temperature SiC and Si_3N_4 materials.

REFERENCES

1. Jacobson, N.S.; Fox, D.S.; and Smialek, J.L.: Molten Salt Corrosion of Silicon Carbide and Silicon Nitride. Environmental Degradation of Engineering Materials III, R.P. McNitt, ed., Penn. State Univ., Apr. 13-17, 1986.

2. Smialek, J.L.; and Jacobson, N.S.: Mechanism of Strength Degradation for Hot Corrosion of α-SiC. J. Am. Ceram. Soc., vol. 69, no. 10, Oct. 1986, pp. 741-752.

3. Jacobson N.S.; Stearns, C.S.; and Smialek, J.L.: Burner Rig Corrosion of SiC at 1000 °C. Adv. Ceram. Mater., vol. 1, no. 2, Apr. 1986, pp. 154-161.

4. Jacobson, N.S.; and Smialek, J.L.: Corrosion Pitting of SiC by Molten Salts. J. Electrochem. Soc., vol. 133, no. 12, Dec. 1986, pp. 2615-2620.

5. Fox, D.S.; Jacobson, N.S.; and Smialek, J.L.: The Molten Salt Corrosion of Silicon Carbide and Silicon Nitride. 24th Automotive Technology Development Contractors Coordination Meeting, Dearborn, MI, DOE/SAE Conf. 861002, 1986.

TABLE I. - COMMERCIAL SiC AND Si_3N_4

A.	SiC	Hexoloy	(Sohio/Carborundum)
B.	SiC	SC 201	(Kyocera)
C.	SiC	β-SiC	(GE)
D.	SiC	KX01	(Sohio/Carborundum)
E.	Si_3N_4	AY6	(GTE)
F.	Si_3N_4	SN50	(NGK)
G.	Si_3N_4		(Toshiba)

ORIGINAL PAGE IS
OF POOR QUALITY

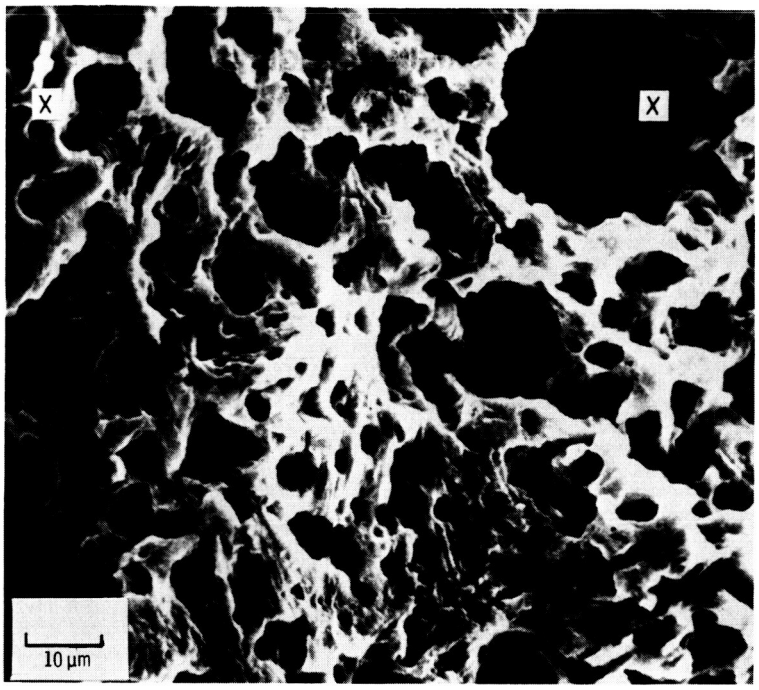

FIGURE 1. - HONEYCOMB PITTING ATTACK MORPHOLOGY AFTER Na_2SO_4/SO_3 CORROSION OF SINTERED SiC (A). (1000 °C, 48 hr, CORROSION PRODUCTS REMOVED BY HF DISSOLUTION.)

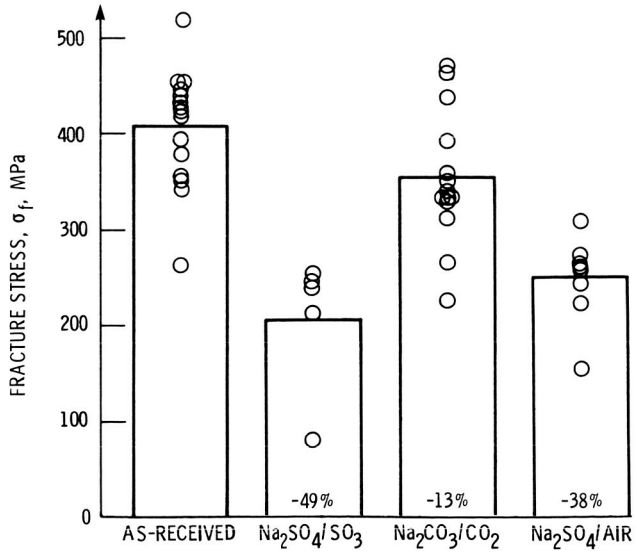

FIGURE 2. - ROOM TEMPERATURE STRENGTH DEGRADATION AFTER FURNACE CORROSION OF SiC (A). (1000 °C, 48 hr.)

ORIGINAL PAGE IS
OF POOR QUALITY

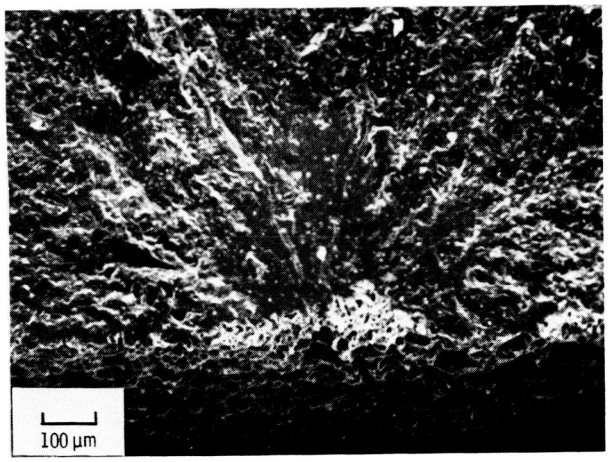

(a) RADIAL CRACK LINES EMANATING FROM PIT.

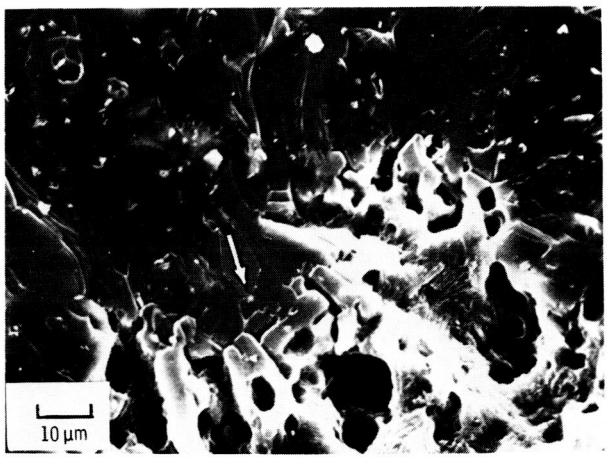

(b) HONEYCOMB NATURE OF PIT.

FIGURE 3. - CORROSION PIT FRACTURE ORIGIN AFTER Na_2SO_4/SO_3 FURNACE CORROSION OF SiC (A). (1000 °C 48 hr, CORROSION PRODUCTS REMOVED BY HF DISSOLUTION.)

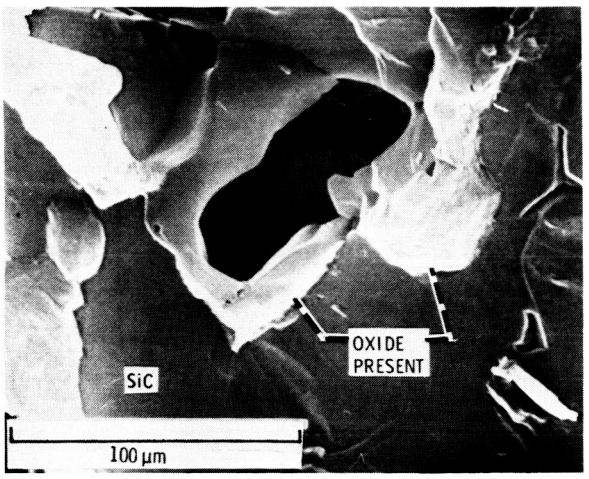

(a) GAS BUBBLE WITHIN SCALE.

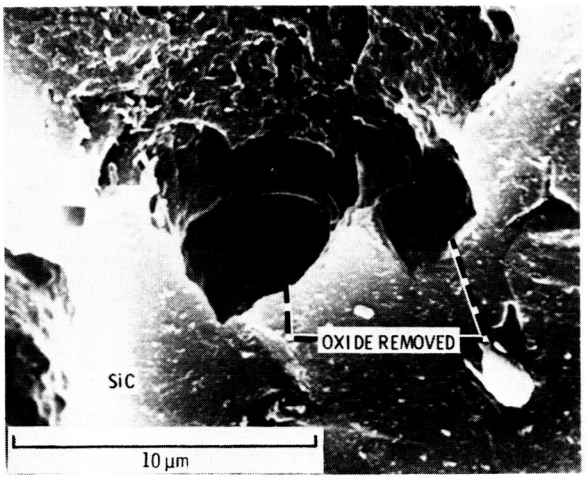

(b) PRODUCTS REMOVED BY HF DISSOLUTION.

FIGURE 4. - DETAIL OF A FRACTURE ORIGIN AT THE SCALE-SiC (A) INTERFACE AFTER Na_2SO_4/SO_3 FURNACE CORROSION. (1000 °C, 48 hr.)

ORIGINAL PAGE IS
OF POOR QUALITY

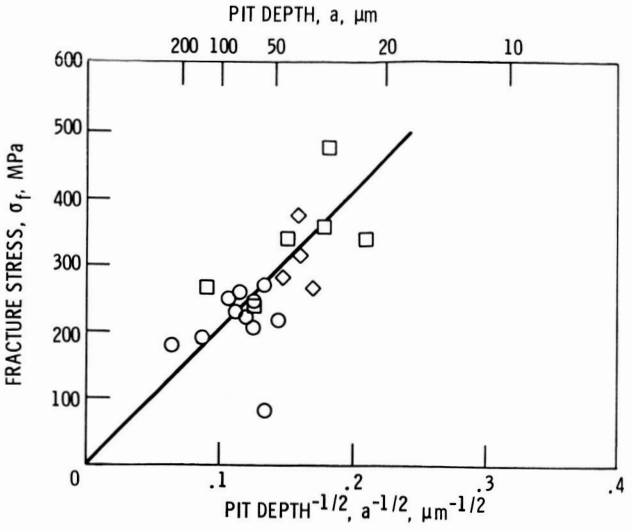

FIGURE 5. - CORRELATION OF FRACTURE STRENGTH WITH CORROSION PIT DEPTH: (○) Na_2SO_4/SO_3, (◇) Na_2CO_3/CO_2, (□) Na_2SO_4/AIR CORROSION. (SiC (A), 1000 °C, 48 hr.)

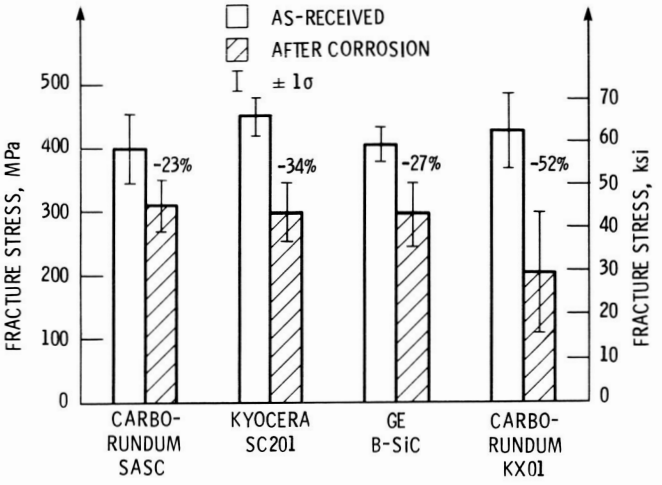

FIGURE 6. - ROOM TEMPERATURE STRENGTH DEGRADATION AFTER BURNER RIG CORROSION OF VARIOUS COMMERCIALLY AVAILABLE SiC MATERIALS (A, B, C, D). (1000 °C, 40 hr, 2 ppm Na.)

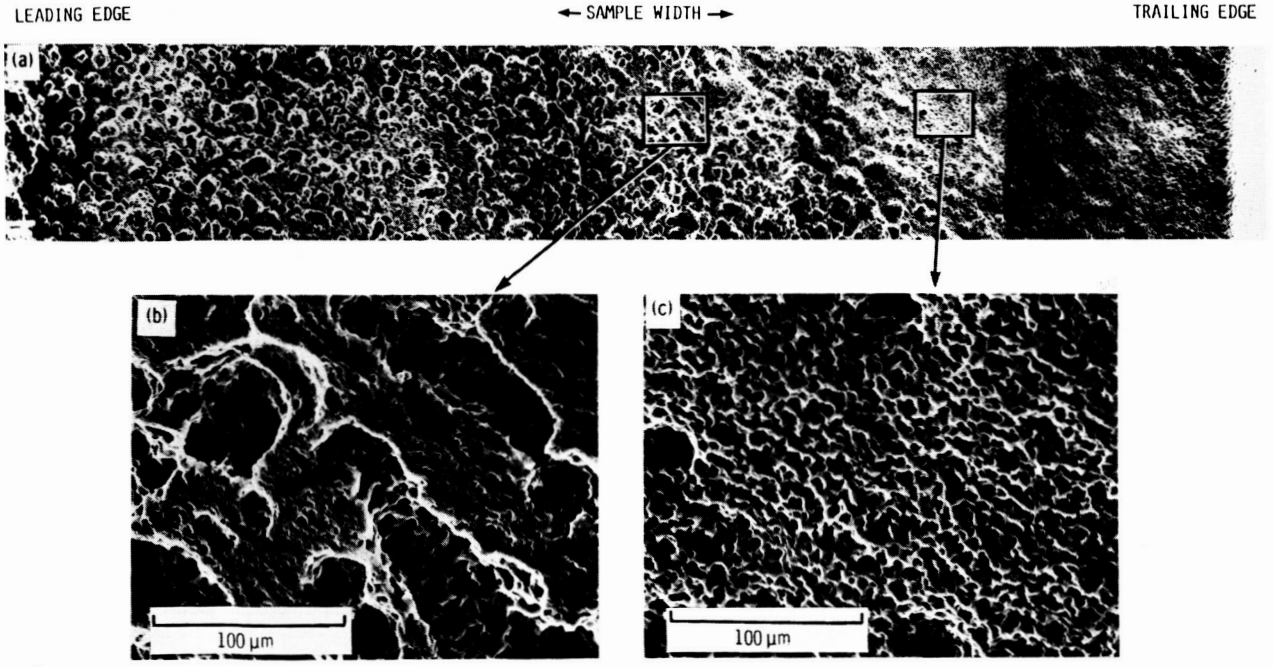

FIGURE 7. - VARIATION IN PITTING MORPHOLOGY FOR BURNER RIG CORRODED SiC (A). (1000 °C, 13.5 hr, 4 ppm Na, CORROSION PRODUCTS REMOVED BY HF.)

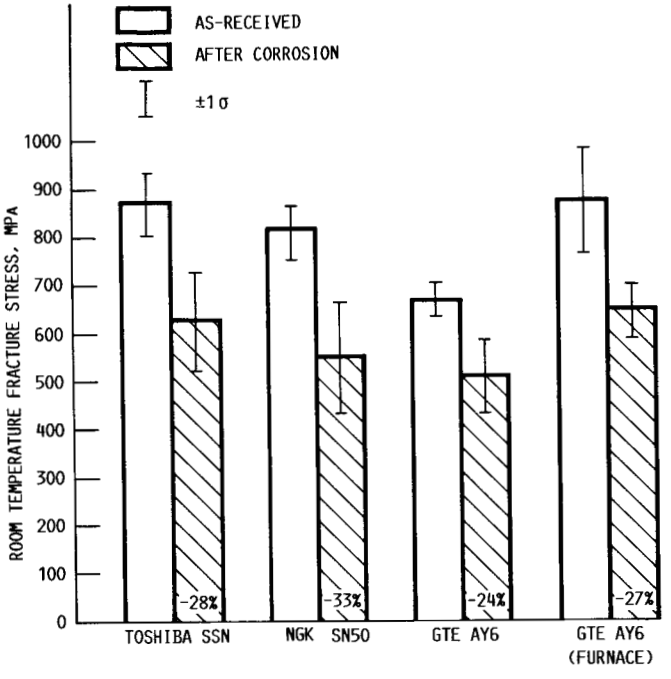

FIGURE 8. - ROOM TEMPERATURE STRENGTH DEGRADATION AFTER BURNER RIG CORROSION OF COMMERCIALLY AVAILABLE Si_3N_4 MATERIALS (E, F, G). (1000 ^{o}C, 40 hr, 2 ppm Na.)

ORIGINAL PAGE IS
OF POOR QUALITY

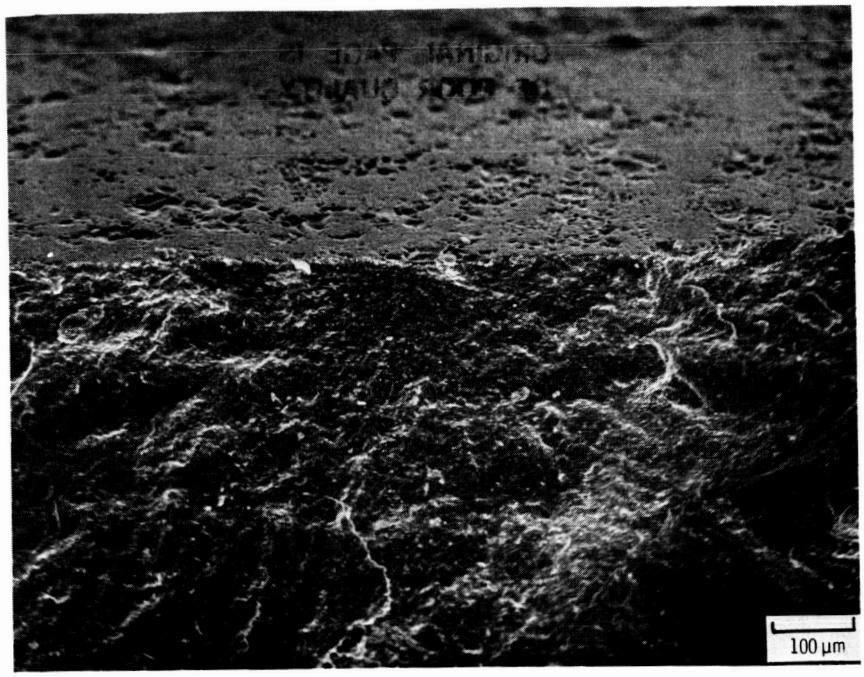

(a) ARRAYS OF BUBBLES EXPOSED ON TOP SURFACE.

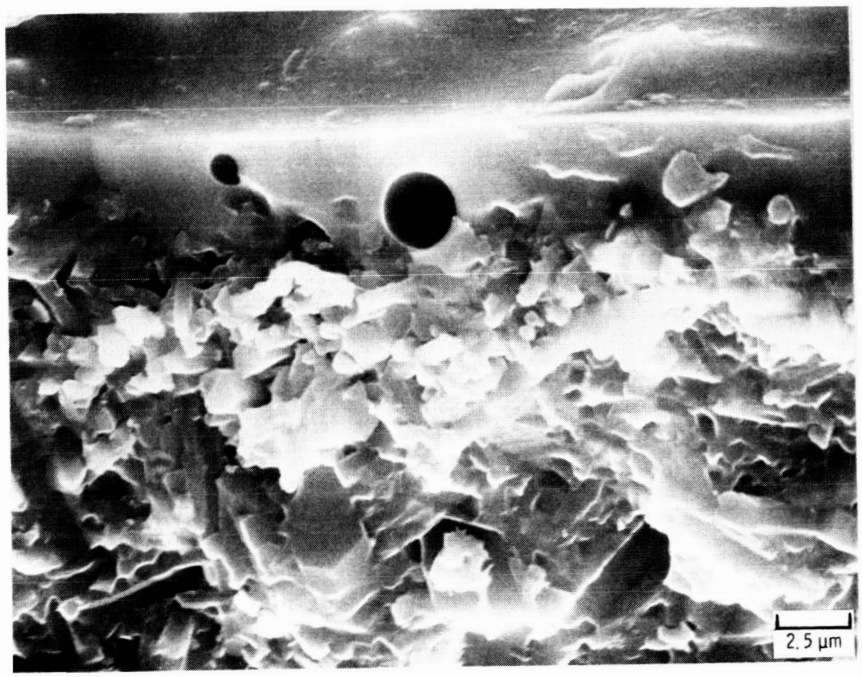

(b) TRAPPED BUBBLES IN SCALE CROSS-SECTION.

FIGURE 9. - FAILURE ORIGIN OF Na_2SO_4/O_2 FURNACE CORRODED Si_3N_4 (E).

ORIGINAL PAGE IS
OF POOR QUALITY

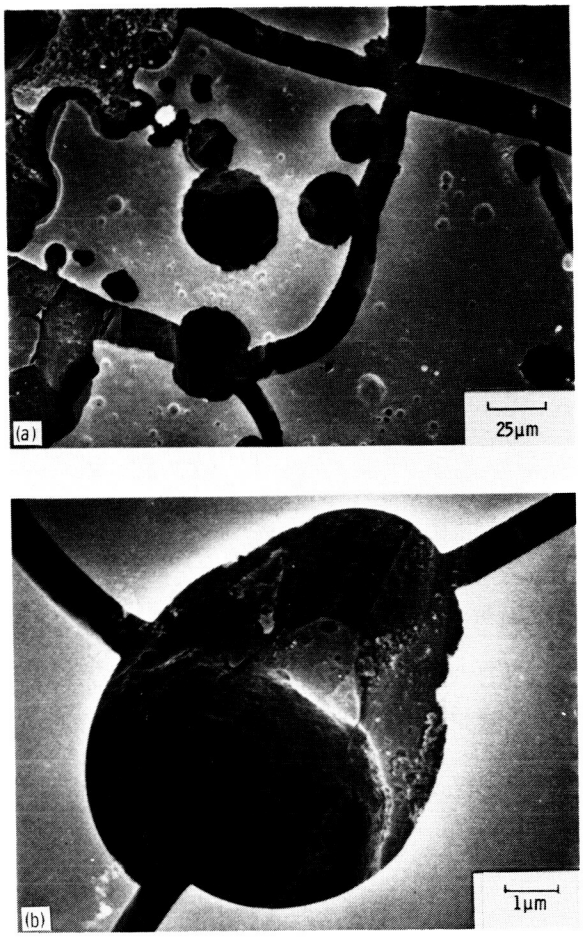

FIGURE 10. - PITTING ATTACK BENEATH PORES IN LOWER SiO_2 LAYER OF CORRODED SiC. (Na_2CO_4/CO_2, 1000 °C, 1 hr, OUTER $Na_2O \cdot xSiO_2$ LAYER DISSOLVED BY H_2O.)

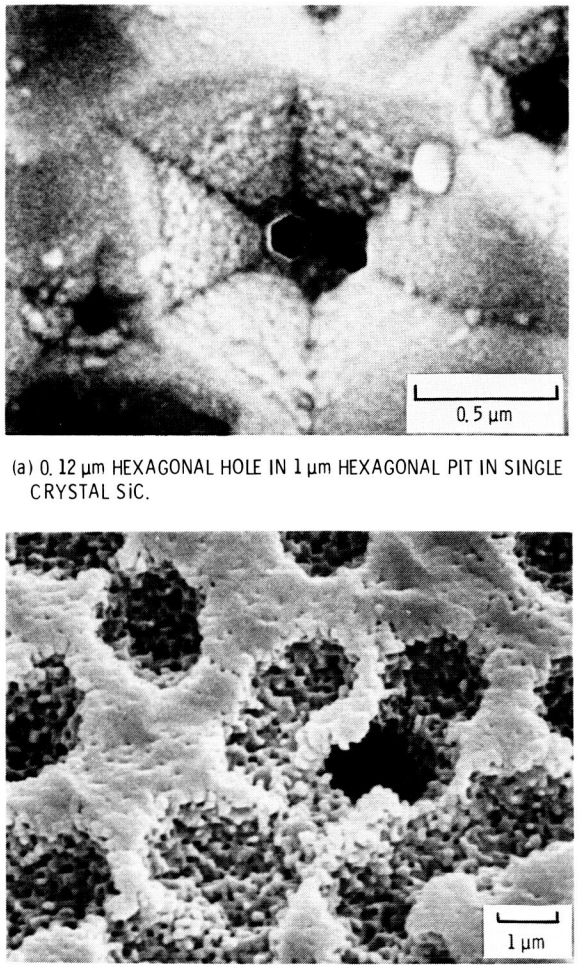

(a) 0.12 μm HEXAGONAL HOLE IN 1 μm HEXAGONAL PIT IN SINGLE CRYSTAL SiC.

(b) TEXTURED PITS IN SINGLE CRYSTAL Si.

FIGURE 11. - CRYSTALLOGRAPHIC PITTING IN SINGLE CRYSTAL SiC AND Si CAUSED BY Na_2CO_3/CO_2 CORROSION. (1000 °C, 20 hr, SCALES REMOVED BY HF DISSOLUTION.)

1. Report No.	2. Government Accession No.	3. Recipient's Catalog No.
NASA TM-89820		

4. Title and Subtitle	5. Report Date
Hot Corrosion Attack and Strength Degradation of SiC and Si_3N_4	6. Performing Organization Code 533-05-11
7. Author(s) James L. Smialek, Dennis S. Fox, and Nathan S. Jacobson	8. Performing Organization Report No. E-3466
	10. Work Unit No.
9. Performing Organization Name and Address National Aeronautics and Space Administration Lewis Research Center Cleveland, Ohio 44135	11. Contract or Grant No.
	13. Type of Report and Period Covered Technical Memorandum
12. Sponsoring Agency Name and Address National Aeronautics and Space Administration Washington, D.C. 20546	14. Sponsoring Agency Code

15. Supplementary Notes

Prepared for Environmental Degradation of Engineering Materials III, sponsored by Pennsylvania State University, University Park, Pennsylvania, April 13-15, 1987.

16. Abstract

Thin films of Na_2SO_4 and Na_2CO_3 molten salt deposits were used to corrode sintered SiC and Si_3N_4 at 1000 °C. The resulting attack produced pitting and grain boundary etching resulting in strength decreases ranging from 15 to 50 percent. Corrosion pits were the predominant sources of fracture. The degree of strength decrease was found to be roughly correlated with the depth of the pit, as predicted from fracture toughness considerations. Gas evolution and bubble formation were key aspects of pit formation. Many of the observations of furnace exposures held true in a more realistic burner rig test.

17. Key Words (Suggested by Author(s))	18. Distribution Statement
Hot corrosion; Molten salts; Silicon carbide; Silicon nitride	Unclassified - unlimited STAR Category 27

19. Security Classif. (of this report)	20. Security Classif. (of this page)	21. No. of pages	22. Price*
Unclassified	Unclassified	11	A02

*For sale by the National Technical Information Service, Springfield, Virginia 22161